Atmospheric Research 266 (2022) 105969

Contents lists available at ScienceDirect

Atmospheric Research

journal homepage: www.elsevier.com/locate/atmosres

Diffuse light around cities: New perspectives in satellite remote sensing of nighttime aerosols

Miroslav Kocifaj [a,b,*], Salvador Bará [c]

[a] ICA, Slovak Academy of Sciences, Dúbravská cesta 9, 845 03 Bratislava, Slovakia
[b] Faculty of Mathematics, Physics, and Informatics, Comenius University, Mlynská dolina, 842 48 Bratislava, Slovakia
[c] Dept. de Física Aplicada, Universidade de Santiago de Compostela, 15782 Santiago de Compostela, Galicia, Spain

ARTICLE INFO

Keywords:
Aerosol remote sensing
Satellite nighttime imagery
Multi-angle radiance data
Diffuse light around cities

ABSTRACT

Satellite remote sensing of nighttime aerosols in the lower atmosphere poses additional challenges in comparison with daytime sensing, due to the specific features of the available light sources and the different scattering geometries. In this work we develop a detailed quantitative model for the top-of-atmosphere radiance of the halos of diffuse light observed around cities in satellite nighttime imagery. It is shown that these scattered light distributions contain relevant information about the aerosol properties, and that under some basic assumptions they can be used to estimate them. We formalize the basis of a method for retrieving the aerosol particle size number distribution function based on inverting the angular dependence of the radiance detected in near-nadir remote sensing observations. The results stress the convenience of endowing future night Earth observation missions with enhanced angular detection capabilities.

1. Introduction

Retrieving information on nighttime aerosols is a challenging task, due to the lack of reliable standard light sources. Aerosol information is needed for basic studies on atmospheric dynamics as well as for many practical applications, as e.g. in light-pollution research to allow for accurate modeling of the propagation of artificial light in the nocturnal environment.

Aerosols are among the most variable atmospheric constituents. They have direct and indirect impacts on the radiative balance of the atmosphere, specifically on the upward and downward radiance at different wavelengths and altitudes. The largest amount of solid and liquid particles reside in the lower troposphere, showing peak concentrations around atmospheric pollution sources. Aerosol envelopes of urban areas could be closely linked to emission sources such as industry, energy production or motor vehicles (Rodrıguez et al., 2004), each producing particulate matter of different sizes, shapes, and material compositions. It is therefore difficult to model the atmospheric radiation budget accurately if the aerosol microphysical properties of the local atmosphere remain unknown.

Mishchenko et al. (2005) summarized the optical parameters of aerosols needed as input to the radiative transfer models. Among them, the aerosol optical depth, AOD, and the scattering phase function, P, are primarily important for solving the inverse scattering problem for diffuse light around cities as observed from satellites. The single scattering albedo (SSA, Spurr, 2006) is of less significance to the problem studied here, since the contribution from aerosols to the detected optical signal scales roughly linearly with SSA. It is well recognized theoretically and experimentally that both, AOD and P, depend strongly on the particle size distribution function, here referred to as f_0. Using the conventional Mie theory the above parameters can be determined by numerical integration of the products of Mie functions and f_0 over the whole range of particle sizes.

The main types of chemical aerosol components are somehow predictable in a regional context since they are related to the local emission sources, either anthropogenic or natural. For instance, mineral dust particles are typically found in desert regions (Krueger et al., 2004), and their refractive indices can be inferred to a certain extent (Lee et al., 2020). However, the size distribution function, f_0, is extremely variable temporally and spatially, and can be scarcely estimated a priori on a regional basis. It is possible, nevertheless, to derive it from spectrally resolved observations. Among the remote sensing products, the AOD database is quite rich (Zhang et al., 2008; Johnson et al., 2013). When determined as a function of wavelength (either from satellite or ground-

* Corresponding author at: ICA, Slovak Academy of Sciences, Dúbravská cesta 9, 845 03 Bratislava, Slovakia.
E-mail address: Miroslav.Kocifaj@savba.sk (M. Kocifaj).

https://doi.org/10.1016/j.atmosres.2021.105969
Received 30 July 2021; Received in revised form 27 November 2021; Accepted 7 December 2021
Available online 11 December 2021

based systems, Dubovik et al., 2019, Sogacheva et al., 2020) the AOD can be interpreted in terms of f_0. The simplest approach is to derive f_0 from the slope of AOD spectra, i.e. from the Ångström exponent (Dhar et al., 2018).

Satellite remote sensing of tropospheric aerosols based on scattered sunlight is a mature and well established technique (Zhang et al., 2021). In contrast, the theoretical development of retrieval methods to characterize aerosols at nighttime is still in its infancy (Wang et al., 2020). This is partly due to the substantially different geometries involved in this problem. Whereas the daytime Sun provides a stable extraterrestrial source of nearly parallel light beams, the nighttime atmosphere is illuminated by myriads of localized ground-based sources (cities or towns) scattered over a large territory.

Most current studies based on city lights take advantage of the detection of their direct radiance, which has been shown to be instrumental for e.g. mapping urban areas or estimating population (Levin et al., 2020). The diffuse halos of light observed around cities in satellite nighttime imagery, in turn, have been much less studied. However, they are an abundant source of complementary information on the atmospheric environment (Kocifaj and Bará, 2020; Sánchez de Miguel et al., 2020). The information that can be retrieved from scattered light is generally large, when compared to the one contained in the direct light emissions, because light scattering data are very sensitive indicators of the particle microphysics. For instance, the phase function $P(\theta)$ at small scattering angles is sensitive to the fluctuation of the content of large particles (Aptowicz et al., 2013), while the radiance recorded at mid-to-large scattering angles is a valuable source of information about the content of small particles. In combination with the spectral dependence of P, particle sizing based on remote sensing of scattered light may benefit of an improved retrieval accuracy. Contrasting to satellite remote sensing methods of daylight clear-sky top-of-atmosphere radiance, the scattering angle of artificial lights at nighttime is not constant for any given direction of observation. The inversion of upward radiance data therefore requires a more conservative approach based on useful approximations, namely limiting the directions of observation to low nadir angles.

In a previous Letter (Kocifaj and Bará, 2020) we reported experimental results showing that the aerosol particle size number distribution function in the air column can be retrieved from angularly resolved measurements of the scattered radiance of the halos surrounding cities at night, as detected by the panchromatic DNB band of the VIIRS on-orbit radiometer on board the Suomi-NPP satellite. The complete physical model underlying this retrieval approach, however, was not fully described in that Letter. Given the significance and the practical usefulness of these results, in the present paper we develop step-by-step this model, in order to make it available for the aerosol remote sensing community at large and to foster the development of new applications in this field. The method allows for extensive aerosol characterization in nighttime, which is an important complement to daytime observations, since both are critically important for understanding the atmospheric processes and specifically the evolution of aerosol composition and concentrations in urban regions.

The structure of this paper is as follows. In Section 2 we develop the basic equations for the radiance at the top of the atmosphere produced by the scattered artificial light emitted from an elementary city area, which is the basic constituent of the halos observed around cities in nightime satellite imagery. We provide simplified equations for near-nadir observations and particular types of emitters, as well as evaluate the relative contributions of the molecular and aerosol scatterings to the total radiance in these observing conditions. In Section 3 we calculate the overall scattered radiance produced by a whole city, and show how its angular distribution as observed from Earth orbiting platforms allows to retrieve the aerosol particle size number distribution function. Supplementary materials contain an in-depth description of how aerosol properties impact satellite radiance data. Additional remarks and conclusions are summarized in Sections 4 and 5, respectively.

2. Methods

2.1. The top-of-atmosphere radiance of the halos of diffuse light around cities

Let us consider the geometry shown in Fig. 1, see also Kocifaj and Bará (2020). Two convenient spherical coordinate reference systems can be defined: one centered at the satellite S, located at $\mathbf{r}_S$, with the polar axis Z oriented toward its nadir (unit vector $\hat{\mathbf{z}}$), and the other centered at any arbitrarily chosen point C within the city, located at $\mathbf{r}_C$, with its polar axis Z' oriented toward the local zenith (unit vector $\hat{\mathbf{z}}'$). For the purposes of the subsequent calculations let us designate as *reference plane* the one containing the unit vectors $\hat{\mathbf{r}}_{CS} = (\mathbf{r}_S - \mathbf{r}_C)/\|\mathbf{r}_S - \mathbf{r}_C\|$ (along the line joining C and S) and $\hat{\mathbf{z}}'$, and as *measurement plane* the one containing the vector $\hat{\mathbf{z}}$ and the unit vector $\hat{\mathbf{r}}_{LOS}$ defined along the radiometer line of sight (LOS). Let us additionally denote by Θ the angle between $\hat{\mathbf{r}}_{CS}$ and the LOS, by z_0 the zenith angle of the satellite as seen from C, and by (z,φ) the nadir angle and the azimuth, repectively, of the LOS as seen from S. Hence $\Theta = cos^{-1}(\hat{\mathbf{r}}_{LOS}\cdot\hat{\mathbf{r}}_{CS})$, $z_0 = cos^{-1}(\hat{\mathbf{z}}'\cdot\hat{\mathbf{r}}_{CS})$, and $z = cos^{-1}(\hat{\mathbf{z}}\cdot\hat{\mathbf{r}}_{LOS})$. λ is the wavelength.

We aim to quantify the top-of-atmosphere (TOA) spectral radiance at the satellite, $R_{Sat}(z,\varphi;\lambda)$ [W·m^{-2}·sr^{-1}·nm^{-1}], due to the atmospheric scattering of the city lights emissions. This radiance is built up from the light scattered by all elementary volumes located along the LOS, like the small cube depicted in Fig. 1. The position of any such element can be parametrized by its height h above the plane tangent to the Earth at the city point C or, equivalently, by its zenith angle z', measured in the city reference frame.

A single-scattering approximation is expected to be adequate for providing accurate results in this calculation (Fig. 2), since in most cases we will be interested in evaluating the radiance for relatively small nadir angles z, when the satellite ground track passes close to the cities, and for moderately thick atmospheres. The plots in Fig. 2 show on a linear scale the first scattering radiance relative to the total radiance both computed for the following model input parameters: λ=589 nm, Henyey-Greenstein phase function (Eq. 23) scaled to the asymmetry parameter of g=0.6, single scattering albedo of aerosols $\tilde{\omega}_A$=0.95 (see Eq. 21), AOD = 0.33, aerosol scale height H_A=2.2 km (Eq. 25), Rayleigh

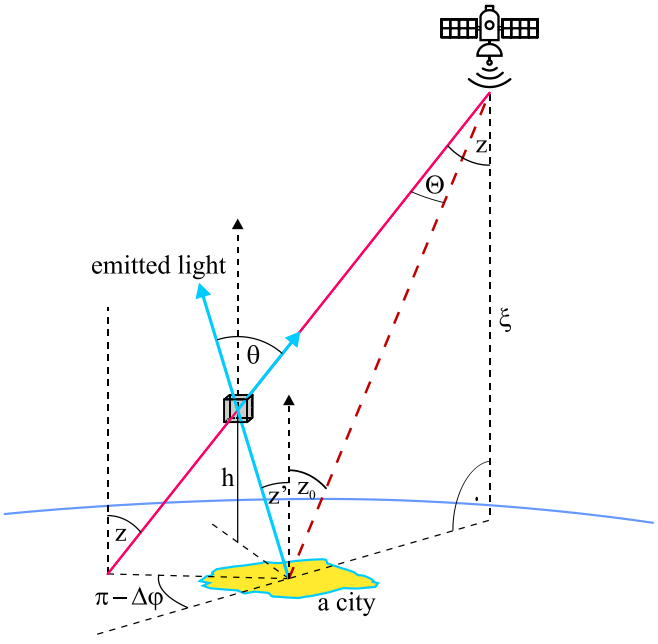

Fig. 1. Geometry of the top-of-atmosphere (TOA) radiance detection of the light scattered by the atmosphere, emitted by a ground-level artificial source.

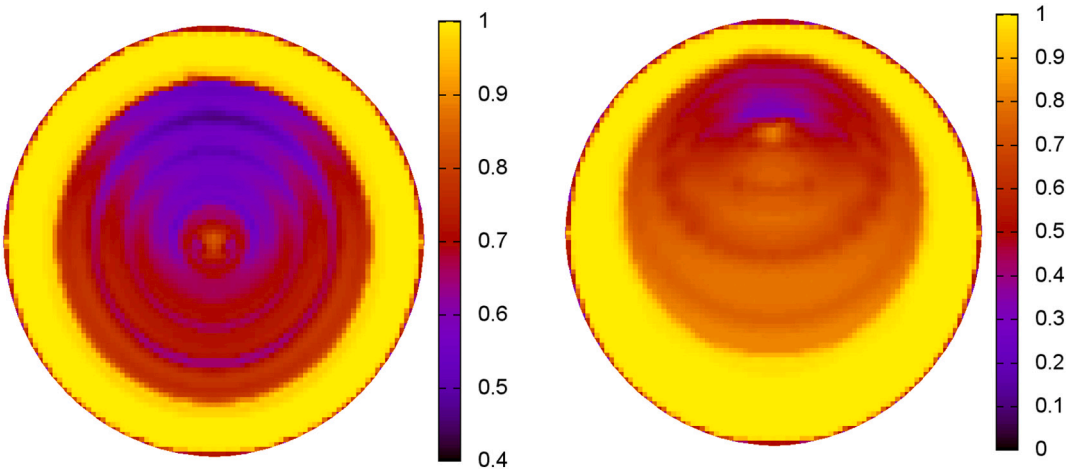

Fig. 2. False color images of $R_{Sat,\ 1}(z,\varphi;\lambda)/R_{Sat}(z,\varphi;\lambda)$ for $\lambda = 589$ nm for an isolated point source of light at ground level (left plot is for nadir view, right plot is for $+45°$ front view). $R_{Sat,\ 1}$ is the theoretical single-scattering contribution to the satellite-recorded radiance, and R_{Sat} is the total radiance, both calculated by using MSOS code (Kocifaj, 2018). The azimuth is measured in a clockwise direction (with north at the top). The zenith and horizon are at the center and the edge of each plot, respectively.

scale height H_M=8.0 km (Aznay et al., 2014). The fractions of the light radiated directly into the upward hemisphere and isotropically reflected from the ground are both 0.1. The upward radiance is computed for an altitude of 72 km, which is high enough for being considered to be the top-of-atmosphere (the concentrations of atmospheric constituents asymptotically approach zero while transitioning to the outer space). One of the interesting findings is that for nadir view the multiple scattering radiance can be important for a wide range of zenith angles (left plot in Fig. 2). It has to be emphasized that single scattering dominance increases in the forward scattering domain and vice versa. Therefore, the optical effects discerned in the left plot of Fig. 2 are most probably due to light beams emitted to low elevations, scattered in the lower atmospheric layer at large angles, while being directed upwards. Due to the same reasons, the multiple scattering may also be relevant to large satellite zenith angles (right plot in Fig. 2), but only for a narrow interval of directions when the line-of-sight passes through the air directly over a bright source of light. However, the intensity of scattered light decays steeply as the angular distance from the light source increases, so the higher scattering orders do not influence the data recorded far from the source (due to the small overall signal), and near to the light source, including a circular ring (a bright halo) around it, by the reasons mentioned above. It has to be emphasized that the yellow rings in Fig. 2 are not an artifact. A distinguishable change from the outer ring to the center appears when transitioning the view from the outer space through the Earth's limb to the Earth itself. The yellow ring is for the view beyond the edge of the physical body of the planet with extremely low intensity of multiply scattered light.

The signal $L_{Sat}(z_s,\varphi_s)$ provided by the detector pointing to the direction (z_s,φ_s) will be

$$L_{Sat}(z_s,\varphi_s) = \int_0^{\infty} S(\lambda)\left[\int_{2\pi} R_{Sat}(z,\varphi;\lambda) f(z,\varphi;z_s,\varphi_s)\ \mathrm{d}^2\alpha\right]\mathrm{d}\lambda \tag{1}$$

where $f(z,\varphi;z_s,\varphi_s)$ is the instrument's field of view weighting function, $S(\lambda)$ is its photometric passband, $\mathrm{d}^2\alpha = \sin z\ \mathrm{d}z\ \mathrm{d}\varphi$ is the solid angle element, and the angular integral is formally extended to the 2π sr front-facing hemisphere, centered on (z_s,φ_s).

In order to evaluate $L_{Sat}(z_s,\varphi_s)$ let us derive first $R_S(z,\varphi) = \mathrm{d}R_{Sat}(z,\varphi;\lambda)$, the contribution to $R_{Sat}(z,\varphi;\lambda)$ due to the emissions of an elementary patch of the city of area dS. The dependence of $R_S(z,\varphi)$ on λ is not explicitly indicated, but shall be kept in mind. Let us further denote by $I_0(z',\phi')$ the spectral radiant intensity [W·sr^{-1}·nm^{-1}] emitted by dS, whose dependence on λ is also implicitly assumed and where (z',ϕ') are the zenith angle and the azimuth, respectively, of the emission directions in the source (city) reference frame (Fig. 1). This spectral radiant intensity can be formally expressed in terms of an equivalent spectral radiance $R_0(z',\phi')$ [W·m^{-2}·sr^{-1}·nm^{-1}], defined as the radiance emitted by a perfectly horizontal surface that would give rise to the same radiant intensity distribution, $I_0(z',\phi')$. Both quantities are related, by definition, as

$$I_0(z',\phi') = R_0(z',\phi')\cos z'\,\mathrm{d}S \tag{2}$$

The radiance $R_0(z',\phi')$ is attenuated along its propagation from the city to the elementary scattering volume at an altitude h above ground level, Fig. 1, according to the Bouguer-Lambert-Beer law. The radiance $R_D(h;z',\phi')$ reaching that volume is:

$$R_D(h;z',\phi') = R_0(z',\phi')\exp\left\{-\frac{1}{\cos z'}\int_0^h k_{ext}(h')dh'\right\} = R_0(z',\phi')\exp\left\{-\frac{\tau(0)-\tau(h)}{\cos z'}\right\} \tag{3}$$

where $k_{ext}(h')$ is the atmospheric volume extinction coefficient [m^{-1}], $\tau(0)$ is the total atmospheric optical thickness at ground level, and $\tau(h)$ is its respective value at altitude h. These functions are also wavelength dependent.

Once the position of the satellite relative to the city and the orientation of the radiometer have been fixed, the direction (z',ϕ') is univocally determined for each value of h along the LOS, so we can denote without loss of information $R_D(h;z',\phi') \equiv R_D(h)$.

Now, the radiant energy [J] incident during a time $\mathrm{d}t$ on the base $\mathrm{d}\sigma$ of the small cube element at h is

$$dQ_D(h) = R_D(h)\ \mathrm{d}\sigma\cos z'\,d\Omega'(h)\ \mathrm{d}t \tag{4}$$

where $\mathrm{d}\Omega'(h) = \mathrm{d}S\cos z'/r'^2 = \mathrm{d}S(\cos z')^3/h^2$ is the solid angle subtended

by the source dS as seen from the elementary atmospheric volume dV = dσ dh. The energy removed from the incident beam within this volume will then be:

$$d^2Q(h) = k_{ext}(h)\frac{dh}{cosz'}dQ_D(h) \tag{5}$$

where the ratio dh/ cos z' is the length of a beam path in dV (Sobolev, 1975).

A fraction of this removed energy is absorbed, and the remaining one is scattered in different directions. The energy $d^2Q_S(h)$ scattered within an elementary solid angle $d\Omega$ [sr] toward the satellite radiometer, at an angle θ with the direction of the incident beam (Fig. 1), is given by:

$$d^2Q_S(h) = d^2Q(h)\,\widetilde{\omega}\,\frac{P(\theta)}{4\pi}d\Omega \tag{6}$$

where $\widetilde{\omega}$ is the atmospheric single scattering albedo, and $P(\theta)$ is the scattering phase function (Kocifaj, 2007). The scattering angle θ is in turn given by

$$cos\theta = coszcosz' + sinzsinz'cos(\varphi - \varphi') \tag{7}$$

where φ' is the aziumuth of the city as seen from the satellite and the other variables have been defined above.

Besides, the solid angle dΩ subtended by the on-orbit radiometer as seen from the scattering volume is dΩ = dA cos z/r^2, where dA is the area element of the radiometer entrance aperture, oriented toward the nadir, and r is the distance from dV to the satellite. Combining Eqs. (3)–(6) we get

$$d^2Q_S(h) = k_{ext}(h)R_0(z',\phi')exp\left\{-\frac{\tau(0)-\tau(h)}{cosz'}\right\}dh\,d\sigma\,d\Omega'(h)\,dt\,\widetilde{\omega}\,\frac{P(\theta)}{4\pi}d\Omega \tag{8}$$

The radiance d$R'_S(h)$ leaving this atmospheric element in the direction of the satellite is then

$$dR'_S(h) \equiv \frac{d^2Q_S(h)}{dt\,d\sigma\,cos\,z\,d\Omega} = k_{ext}(h)R_0(z',\phi')exp\left\{-\frac{\tau(0)-\tau(h)}{cosz'}\right\}\frac{dh}{cos\,z}\,d\Omega'(h)\,\widetilde{\omega}\,\frac{P(\theta)}{4\pi} \tag{9}$$

which will arrive to the satellite attenuated according to the Bouguer–Lambert–Beer law as

$$dR_S(h) \equiv exp\left\{-\frac{1}{cosz}\int_h^{\xi}k_{ext}(h')dh'\right\}dR'_S(h) = exp\left\{-\frac{\tau(h)}{cosz}\right\}dR'_S(h) \tag{10}$$

where ξ is the satellite altitude. Finally, the radiance at the detector due to the sources in dS, $R_S(z,\varphi)$, will be given by the integral of the contributions (9) from all atmospheric elements along the LOS with altitudes from 0 to ξ,

$$R_S(z,\varphi) = \int_{h=0}^{\xi} dR_S(z) = \int_{h=0}^{\xi} exp\left\{-\frac{\tau(h)}{cosz}\right\}dR'_S(h) \tag{11}$$

explicitly:

$$R_S(z,\varphi) = \frac{1}{cos\,z}\int_{h=0}^{\xi} R_0(z',\phi')exp\left\{-\frac{\tau(h)}{cosz}-\frac{\tau(0)-\tau(h)}{cosz'}\right\}\widetilde{\omega}\,k_{ext}(h)\,\frac{P(\theta)}{4\pi}\,d\Omega'(h)dh \tag{12}$$

or, taking into account that $d\Omega'(h) = dS(cosz')^3/h^2$

$$R_S(z,\varphi) = \frac{dS}{cosz}\int_{h=0}^{\xi} R_0(z',\phi')exp\left\{-\frac{\tau(h)}{cosz}-\frac{\tau(0)-\tau(h)}{cosz'}\right\}\widetilde{\omega}k_{ext}(h)\frac{P(\theta)}{4\pi}\frac{cos^3z'}{h^2}dh \tag{13}$$

Substituting Eq. (2) into Eq. (13) in order to express the city emissions in terms of their radiant intensity, $I_0(z',\phi')$, we get

$$R_S(z,\varphi) = \frac{1}{cosz}\int_{h=0}^{\xi} I_0(z',\phi')exp\left\{-\frac{\tau(h)}{cosz}-\frac{\tau(0)-\tau(h)}{cosz'}\right\}\widetilde{\omega}k_{ext}(h)\frac{P(\theta)}{4\pi}\frac{cos^2z'}{h^2}dh \tag{14}$$

Eq. (14) is the basic equation of this model (Eq. (1) in Kocifaj and Bará (2020)). Let us recall that $R_S(z,\varphi)$ is the spectral radiance at the satellite, so that the detector signal will be given by the integral of this radiance within the field of view and the spectral passband of the instrument, as indicated above.

Eq. (14) can be rewritten in terms of other convenient angular quantities like Θ, the angle between the LOS and the city as seen from the radiometer. Denoting by S the position of the satellite, by C that of the city and by O that of the scattering volume, basic trigonometry shows (Fig. 1) that

$$\frac{\left|\overrightarrow{CO}\right|}{sin\Theta} = \frac{\left|\overrightarrow{CS}\right|}{sin(\pi-\theta)} = \frac{\left|\overrightarrow{CS}\right|}{sin\theta}, cosz_0 = \frac{\xi}{\left|\overrightarrow{CS}\right|}, sin\left(\frac{\pi}{2}-z'\right) = cosz' = \frac{h}{\left|\overrightarrow{CO}\right|} \tag{15}$$

so that

$$h = \frac{\xi sin\Theta\,cosz'}{sin\theta cosz_0} \tag{16}$$

and hence

$$R_S(\Theta,\varphi) = \frac{cos^2 z_0}{(\,\xi sin\Theta\,)^2 cos\ z} \int_{h=0}^{\xi} I_0(z',\phi') exp\left\{ -\frac{\tau(h)}{cosz} - \frac{\tau(0)-\tau(h)}{cosz'} \right\} \widetilde{\omega}\, k_{ext}(h)\ \frac{P(\theta)}{4\pi}\ sin^2\theta \mathrm{d}h \tag{17}$$

where $z = z(\Theta, z_0)$.

2.2. Near-nadir observations and particular kinds of emitters

Several useful simplifications can be made in Eq. (17) for observations carried out at very small nadir angles, with the satellite ground-track passing very close to the city ($\Theta, z_0, z \ll 1\ rad$). Observations at small Θ angles are particularly relevant for our purposes, since the radiance of the halos of the city lights, as seen from orbit, decays at a fast rate as the LOS points away from the city borders (Kocifaj and Bará, 2020). For observations made when the satellite is close to the vertical of the city ($z_0 \to 0$) we have

$$cosz \approx cosz_0 \approx 1, \theta \approx z', z \approx \Theta \tag{18}$$

whence

$$R_S(\Theta,\varphi) = \frac{1}{(\,\xi sin\Theta\,)^2} \int_{h=0}^{\xi} I_0(z',\phi') exp\left\{ -\tau(h) - \frac{\tau(0)-\tau(h)}{cosz'} \right\} \widetilde{\omega}\, k_{ext}(h)\ \frac{P(z')}{4\pi}\ sin^2 z'\, \mathrm{d}h \tag{19}$$

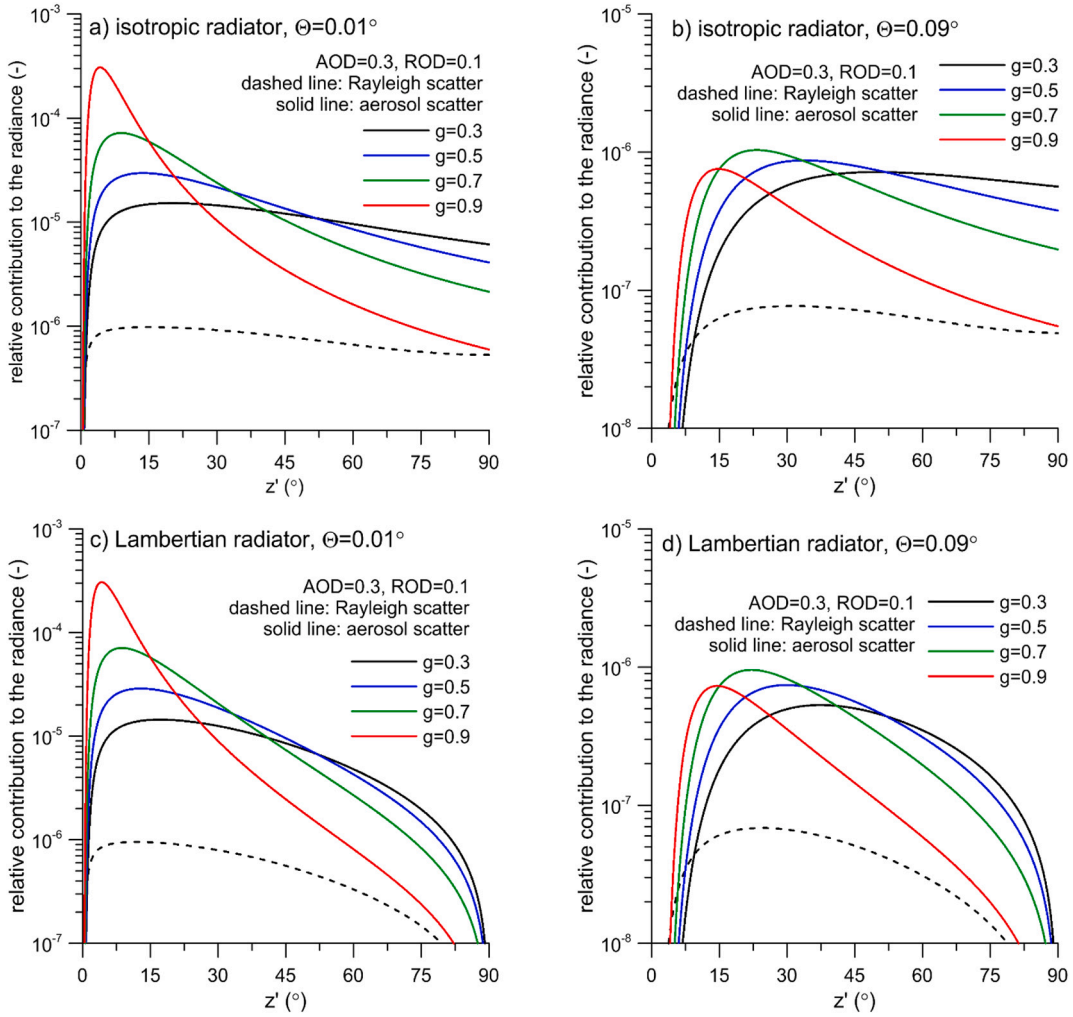

Fig. 3. Relative contribution of aerosols (solid lines) and air molecules (dashed line) to the $R_S(\Theta)$ near-nadir radiance at satellite level (in arbitrary units, per unit dz' interval). AOD = 0.3 (aerosol optical depth), ROD = 0.1 (Rayleigh optical depth), g = aerosol asymmetry parameter. Plots in the top are for isotropic radiators (corresponding to Fig. 2 in Kocifaj and Bará (2020)), while plots in the bottom are for Lambertian sources. From left to right Θ = 0.01°, and 0.09°.

Eq. (19) can be further simplified for the case of azimuthally symmetric emitters, that is, cities whose emitted radiant intensity may depend on the zenith angle z', but not on the azimuth ϕ', so that $I_0(z',\phi') \equiv I_0(z')$. Whereas this emission pattern does not hold, in general, for individual streetlights, it describes satisfactorily the aggregated emissions of multiple light sources in cities with no strong directional preference of the road network. For the sake of simplicity we will assume henceforth that the cities emit with azimuthal symmetry, although evaluating numerically the outcomes of more general intensity radiation patterns would pose no essential difficulty.

Two particular cases of azimuthally symmetric emitters provide useful insights about the behavior of the radiance of the halos around cities at night: the isotropic radiators, whose intensity is constant for all directions of the upper hemisphere, $I_0(z',\phi') = I_0$, and the Lambertian ones, whose equivalent radiance is constant, $R_0(z',\phi') = R_0$, and hence $I_0(z',\phi') = I_0 \cos z'$. Both will be analyzed in the sections below.

2.3. Relative contributions of molecular and aerosol scattering

The scattering process is accounted for in (17) through the term $\widetilde{\omega}\, k_{ext}(h)P(\theta)/4\pi$, which, written in that form, assumes that the concentration profile of the scatterers and the relative angular distribution of the scattered light are independent functions. In case of having N kind of scatterers, characterized by different albedos $\widetilde{\omega}_i$, atmospheric concentration profiles $k_{i,\,ext}(h)$ and scattering phase functions $P_i(\theta)$, $i = 1, \ldots, N$, the term above shall be replaced by a sum over classes

$$\widetilde{\omega}k_{ext}(h)\frac{p(\theta)}{4\pi} \rightarrow \frac{1}{4\pi}\sum_{i=1}^{N}\widetilde{\omega}_i k_{i,ext}(h)P_i(\theta) \tag{20}$$

In our case we have to account for the aggregated contributions of the molecular (M) and aerosol (A) components of the atmosphere,

$$\widetilde{\omega}k_{ext}(h)\frac{p(\theta)}{4\pi} \rightarrow \frac{1}{4\pi}\left[\widetilde{\omega}_M k_{M,ext}(h)P_M(\theta) + \widetilde{\omega}_A k_{A,ext}(h)P_A(\theta)\right] \tag{21}$$

The molecular scattering follows a Rayleigh behavior, with molecular albedo $\widetilde{\omega}_M \cong 1$, and a scattering phase function given by

$$P_M(z') = \frac{3}{4}\left(1 + cos^2 z'\right) \tag{22}$$

Aerosols, in turn, have a wider range of albedos, and their scattering phase function shall generally be calculated using the exact Mie theory (as we will do in Section 3.2). But very often, and in particular for the purposes of our present calculation, $P_A(z')$ can be successfully approximated by the well-known Henyey–Greenstein function

$$P_A(z') = \frac{1 - g^2}{(1 + g^2 - 2gcosz')^{3/2}} \tag{23}$$

where g, $(-1 \le g \le 1)$, is the asymmetry parameter. The volume extinction coefficients $k_{i,\,ext}(h)$ and their associated atmospheric optical depths $\tau_i(h)$, $i \in \{M, A\}$, for an adiabatic atmosphere have the form

$$k_{i,ext}(h) = \frac{\tau_{i,0}}{H_i}e^{-h/H_i}, \tau_i(h) = \tau_{i,0}e^{-h/H_i} \tag{24}$$

where $\tau_{i,\,0}$ is the optical depth corresponding to one airmass (i.e. from ground-level, $h = 0$), and H_i is the characteristic scale height of the exponential concentration profile of each kind of scatterers. So we have:

It is now convenient to assess whether this formula could be further simplified, by examining the relative contributions of the molecular and aerosol scatterers to the overall value of $R_S(\Theta,\varphi)$, the near-nadir TOA radiance. Since the order of magnitude of the results is only weakly dependent on the particular shape of the city radiant intensity emission pattern, we can make the evaluation for an isotropic emitter $I_0(z',\phi') = I_0$. Note that for observations made with the city at the nadir of the satellite, assuming azimuthally symmetric emitters, the TOA radiance is independent from the azimuth angle φ, and hence $R_S(\Theta,\varphi) = R_S(\Theta)$.

As shown in Figs. 3–5, the contribution of Rayleigh scattering to the nadir radiance at the satellite is marginal for $\Theta \le 0.09°$. Outside this range of angles the radiance of the city halos detected from Earth orbit normally approaches that of the dark background, as measured currently operative spaceborne radiometers. The data in Figs. 3–5 (except for Fig. 4a) are shown as density functions with respect to the altitude above the source of light or the zenith angle of the emitted light. The integral of a specific density function over the entire range of its variable is proportional to the total radiance at the satellite level. The contributions from aerosols and air molecules are shown separately and proportionally to their actual impact. To understand better Figs. 3 and Figs. 4b,d we highlight that very low zenith angle z' means high-altitude light scattering (consult Fig. 4a). Light scattering by aerosol particles from upper altitudes is so small because the concentration of particulate matter is extremely low tens of kilometers above the ground level. This is why, the aerosol-component of scattered light falls off very fast as z' approaches zenith. The ratio of aerosol to molecular concentration is proportional to $\exp\{-hH_A^{-1} + hH_M^{-1}\}$. The aerosol content relative to the concentration of air molecules is reduced 20-times when transitioning from h = 1 km to h = 10 km (z'=8.2° to 0.82° for Θ=0.01°).

Fig. 3 shows how efficiently the light emitted toward z' contributes to the optical signal captured by satellite at two nadir directions, Θ=0.01° and Θ=0.09°. The light beams propagating through the atmosphere with very inclined trajectories are increasingly important at larger Θ when aerosol particles are small in size or have g<0.3. It is well known from light scattering theories that g quickly approaches zero when the characteristic particle sizes are much smaller than λ (most of particles with sizes at least 10× smaller than the wavelength often have g<0.1; Moosmüller and Ogren, 2017, Videen et al., 1998). Such aerosol particles tend to scatter more uniformly, with only a slight intensity enhancement in the forward direction. Due to their increased ratio of side-to-forward scattering efficiency, small particles can make the halo of diffuse light around a city more extense. However, most aerosol particles do have g>0.5 (Pandolfi et al., 2018) and most typically g≈0.7 in the visible spectrum (see e.g. tables 4–5 and 7 in Horvath et al., 2002 and the statistics in the top of Fig. 1 in Liu et al., 2008). A process of humidification in wet air is further associated with a rapid increase of size and water content of aerosol particles (Fig. 1 in Zhang et al., 2012), resulting in a continuous increase of g. It has been shown by Hartley and Hobbs (2001) that dry aerosols with g≈0.5 can become strongly forward-scattering (g≈0.8) under high relative humidity conditions. The computations made for g=0.3 and g=0.9 in Figs. 3–5 therefore represent the lower and the upper bounds we can expect from various aerosol systems. We assume that plots for g=0.7 best approximate natural conditions in urban and rural contexts.

It can be seen in Fig. 3 that the peak contribution to the total radiance at satellite level comes from light emissions directed nearly upwards, a fact more apparent for Lambertian than for isotropic sources (compare

$$R_S(\Theta,\varphi) = \frac{1}{4\pi(\,\xi sin\Theta\,)^2}\int_{h=0}^{\xi} I_0(z',\phi')\left[H_M{}^{-1}\tau_M(h)P_M(\theta) + \widetilde{\omega}_A H_A{}^{-1}\tau_A(h)P_A(\theta)\right] exp\left\{-\tau(h) - \frac{\tau(0)-\tau(h)}{cosz'}\right\} sin^2 z'\,dh \tag{25}$$

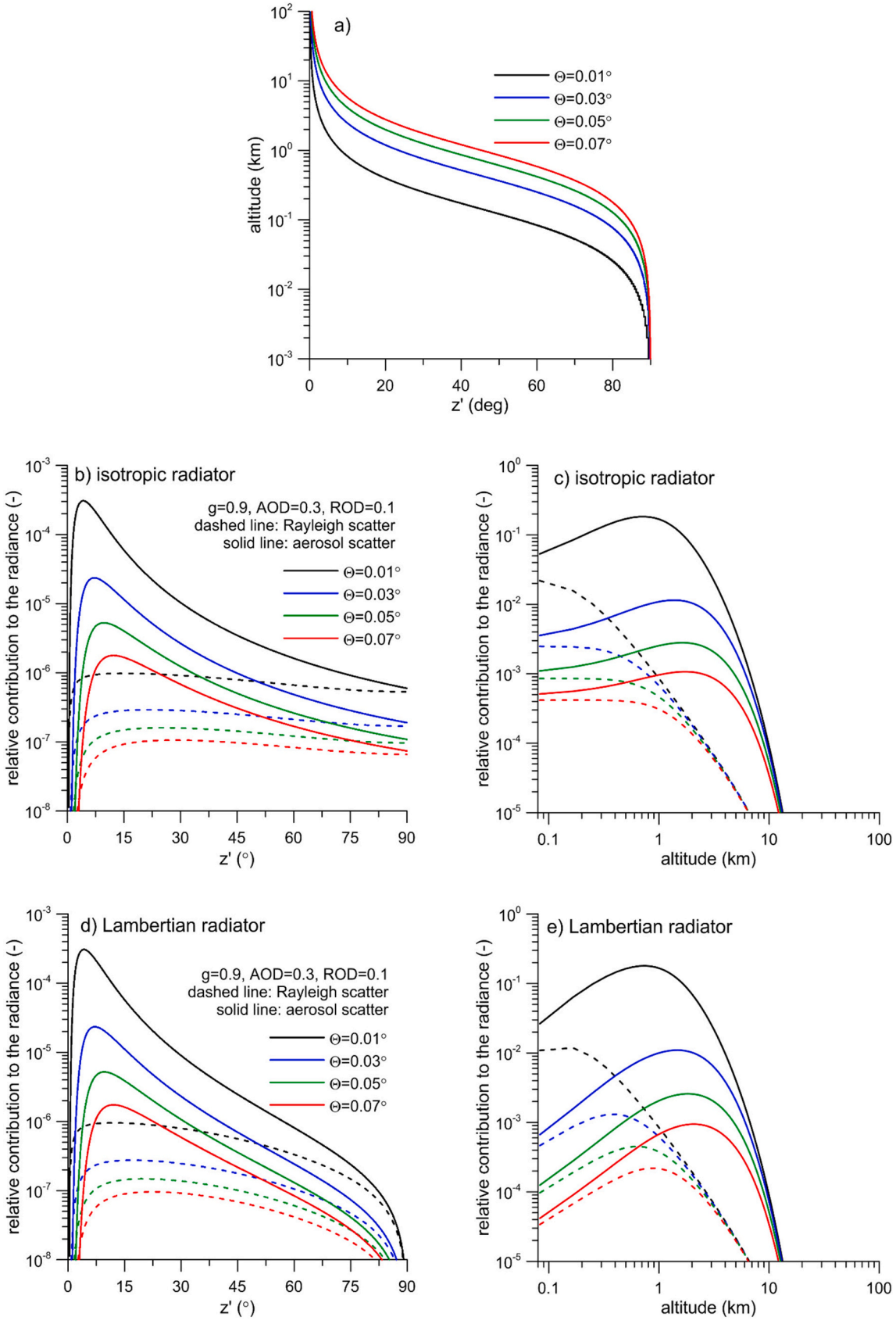

Fig. 4. Top: conversion from z' (°) to h (km) and vice versa. Middle left: aerosol (solid lines) and molecular (dashed lines) relative contributions to the near-nadir radiance at satellite level $R_S(\Theta)$ in function of z', per unit dz' interval, for observation angles $\Theta = 0.01°, 0.03°, 0.05°, 0.07°$, with AOD = 0.3, ROD = 0.1 and g=0.9. Middle right: the same as the latter plot but shown as a function of the altitude h, per unit dh interval. Both plots are for an isotropic light source. Bottom: the same as in middle but for a Lambertian radiator.

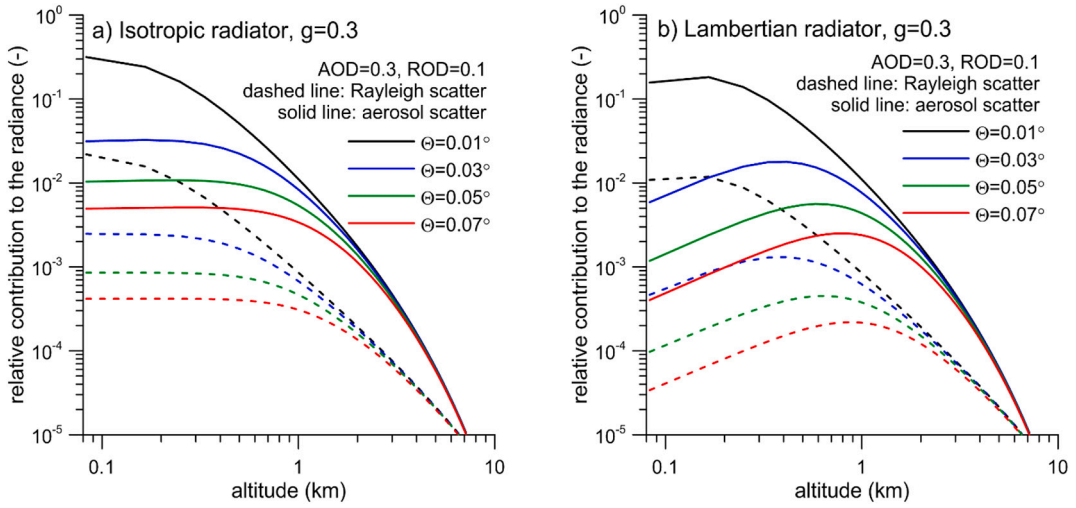

Fig. 5. Relative contributions of aerosol (solid lines) and molecules (dashed lines) to the near-nadir radiance at satellite level, $R_S(\Theta)$, per unit dh interval,for weakly asymmetric aerosol scattering (g=0.3), observation angles $\Theta = 0.01°, 0.03°, 0.05°, 0.07°$, AOD = 0.3 and ROD = 0.1.

top and bottom panels in Fig. 3). The forward-lobed shape of the aerosol scattering patterns (typical for large values of g) strongly supports the dominance of the zenith emissions in the nadir radiance detected at Earth orbit, independently from whether the ground-based light source acts as an isotropic or a Lambertian radiator (see Fig. 4b and d).

It is worthwhile to emphasize that for emissions in different directions the scattering event occurs at different altitudes, subject to the geometrical configuration shown in Fig. 1. The conversion from altitude (h) to zenith angle (z') and vice versa is straightforward, as depicted in

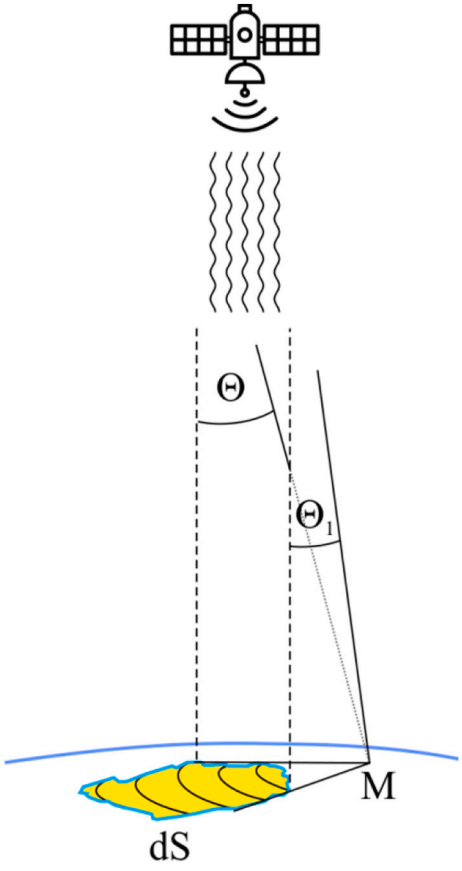

Fig. 6. Angle definitions for the calculation of the TOA radiance due to a city (see also Fig. 1 in Kocifaj and Bará (2020)).

Fig. 4a for a set of satellite observing directions (Θ). This allows to identify the atmospheric layers that most contribute to the satellite radiance, assuming that the light source is an isotropic (Fig. 4c) or a Lambertian (Fig. 4e) emitter. In both cases, the most important contributor turns out to be the light scattered in the lower troposphere, up to 5 km above ground level. This is mostly due to the exponential stratification of the atmospheric constituents (aerosols and air molecules). The smaller g, the larger fraction of photons is removed from the forward direction, which leads to the increased importance of light scattering in the lowest atmospheric layers (compare Figs. 5 and 4).

According to these results, for near-nadir observations of isotropic emitters the molecular (Rayleigh) term can be dropped from Eq. (19), and

$$R_{S,iso}(\Theta) = \frac{I_0 \widetilde{\omega}_A H_A^{-1}}{4\pi(\,\xi sin\Theta\,)^2} \int_{h=0}^{\xi} \tau_A(h) P_A(\theta) exp\left\{ -\tau(h) - \frac{\tau(0)-\tau(h)}{cosz'} \right\} sin^2 z' \mathrm{d}h \tag{26}$$

In an analogous way, for Lambertian cities ($I_0(z', \phi') = I_0 \cos z'$) we have

$$R_{S,Lam}(\Theta) = \frac{I_0 \widetilde{\omega}_A H_A^{-1}}{4\pi(\xi sin\Theta)^2} \int_{h=0}^{\xi} \tau_A(h) P_A(\theta) exp\left\{ -\tau(h) - \frac{\tau(0)-\tau(h)}{cosz'} \right\} cosz' sin^2 z' \mathrm{d}h \tag{27}$$

For predominantly forward-peaked scatterers ($g \gtrapprox 0.6$) the main contributions to the TOA radiance at small observation angles Θ come from the emissions at small zenith angles z' (Fig. 1), so we can set $\cos z' \approx 1$ for both isotropic and Lambertian emitters:

$$R_S(\Theta) = \frac{I_0 \widetilde{\omega}_A H_A^{-1} exp\{-\tau(0)\}}{4\pi(\,\xi sin\Theta\,)^2} \int_{h=0}^{\xi} \tau_A(h) P_A(\theta) sin^2 z' \mathrm{d}h \tag{28}$$

3. Results

3.1. Overall scattered radiance produced by a city

The equations developed in Section 2 provide the scattered TOA radiance at the satellite due to the emissions of a small patch of the city, of area dS, centered at the point $\mathbf{r}_C$. The element of area dS is implicitly contained in the main equation of the model for $R_S(z, \varphi)$, Eq. (14), and in its particularization for near-nadir observation angles, $R_S(\Theta, \varphi)$, Eq. (25), through the radiant intensity function $I_0(z', \phi')$, which is proportional to

dS (see Eq. 2). In order to evaluate the total scattered radiance at the satellite, $R_{Sat}(z,\varphi;\lambda)$, we have to add the contributions of all dS elements of the urban light emission region, Σ_s.

In order to do so, let us remind that

$$R_{Sat}(z,\varphi;\lambda) = \int_{\Sigma_s} \mathrm{d}R_{Sat}(z,\varphi;\lambda) \tag{29}$$

where $\mathrm{d}R_{Sat}(z,\varphi;\lambda) \equiv R_S(\Theta,\varphi)$, and that we can write the radiant intensity in terms of an effective radiance as $I_0(z',\phi') = R_0(z',\phi')\cos z'\,\mathrm{d}S$. Additionally, the general equation of the model for near-nadir angles, Eq. (25) can be rewritten as:

$$R_S(\Theta,\varphi) = \frac{1}{4\pi(\,\xi sin\Theta\,)^2} F(\Theta,\varphi)\,\mathrm{d}S \tag{30}$$

where

$$F(\Theta,\varphi) = \int_{h=0}^{\xi} R_0(z',\phi')\mathrm{d}S\left[H_M{}^{-1}\tau_M(h)P_M(\theta) + \widetilde{\omega}_A H_A{}^{-1}\tau_A(h)P_A(\theta)\right] exp\left\{-\tau(h) - \frac{\tau(0)-\tau(h)}{cosz'}\right\} cosz' sin^2 z'\,\mathrm{d}h \tag{31}$$

for the general case, with immediate particularizations for the simplified conditions described in Eqs. (26)–(28). So we have,

$$R_{Sat}(z,\varphi;\lambda) = \int_{\Sigma_s} \frac{1}{4\pi(\,\xi sin\Theta\,)^2} F(\Theta,\varphi)\,\mathrm{d}S \tag{32}$$

In order to evaluate Eq. (32) we can add the contributions of the sources contained within rings of increasing angular radii Θ (Fig. 6). Denoting by r the distance on the ground from the satellite nadir to the points located at an angular distance Θ, where $r = \xi\tan\Theta \cong \xi\Theta$, the area of a ring of this radius and width $dr \cong \xi\mathrm{d}\Theta$ is $2\pi r\mathrm{d}r = 2\pi\xi^2\Theta\mathrm{d}\Theta$. Only some fraction of this ring will be populated with light sources (see e.g. the arc elements of limited extent in Fig. 6). We can parametrize it by substituting π by a Θ-dependent function $\epsilon(\Theta)$, such that $0 \le \epsilon(\Theta) \le \pi$, and hence $\mathrm{d}S = 2\epsilon(\Theta)\xi^2\Theta\mathrm{d}\Theta$. For instance, for an ideal circular city of radius R whose minimum distance from the edge to the satellite nadir is x we have $r \in [x, 2R + x]$, and

$$\epsilon(\Theta) = cos^{-1}\left[\frac{r^2 + (R+x)^2 - R^2}{2r(R+x)}\right] \cong cos^{-1}\left[\frac{\xi^2\Theta^2 + (R+x)^2 - R^2}{2(R+x)\xi\Theta}\right] \tag{33}$$

Other light source distributions will be associated with their own $\epsilon(\Theta)$, that can be calculated either analytically or numerically, depending on the cases. So, Eq. (32) becomes:

$$R_{Sat}(z,\varphi;\lambda) = \frac{1}{2\pi}\int_{\Theta_1}^{\Theta_2} \frac{\epsilon(\Theta)}{\Theta} F(\Theta,\varphi)\,d\Theta \tag{34}$$

where we have again made use of $\sin\Theta \cong \Theta$.

It has been shown above that for low values of z' the scattered light from aerosol particles dominates the molecular one. The same applies to small observation angles Θ, and also to larger values of z' in case the aerosol asymmetry parameter approaches unity (>0.9). Increasing Θ the contribution from Rayleigh scattering to the satellite radiance also increases, especially when the value of $2\epsilon(\Theta)r = 2\epsilon(\Theta)\xi\Theta$ increased too. For a finite-sized city $\epsilon(\Theta)$ is a unimodal function, i.e. it increases with $r = \xi\Theta$ until the peak value of $\epsilon(\Theta)$ is attained for a specific value of r. Then $\epsilon(\Theta)$ quickly decreases for larger r. This is why distant parts of a city (i.e. lit areas at the opposite edge of the city as seen from the satellite nadir) tend to make relatively small contributions to the overall radiance detected at small nadir angles.

3.2. Estimation of the particle size number distribution function

The main aim of this work is to take advantage of the measured shape of $R_{Sat}(z,\varphi;\lambda)$ to get information about the scatterers present in the air column, and in particular to determine the particle size number distribution function, $f(a,h)$, where $f(a,h)\mathrm{d}a$ is the number of particles per unit volume having radii between a and $a + \mathrm{d}a$ at height h above ground level.

We develop here the explicit model for Lambertian emitters at small nadir angles (up to roughly 30°) and with predominantly forward-peaked aerosol scatterers, Eq. (28). The scattering phase function in the Mie formalism is (Deirmendjian, 1969)

$$P_A(z') = \frac{4\pi}{\widetilde{\omega}_A k_{A,ext}(h)}\left(\frac{\lambda}{2\pi}\right)^2 \int_{a=0}^{\infty} S_{11}(a,z')\,f(a,h)\,da \tag{35}$$

It has to be emphasized that the formula $k_{A,\,ext}(h) \propto e^{-h/H_A}$ is related to the exponential form of $f(a,h) = f(a,0)\,e^{-h/H_A} = f_0(a)\,e^{-h/H_A}$. Note that $f(a,h)$ has dimension m^{-4} and $k_{A,\,ext}(h) = H_A{}^{-1}\tau_A(h)$. Additionally, we know from light scattering theory (McCartney, 1977, Eq. 6–3) that:

$$\widetilde{\omega}_A k_{A,ext}(h) = k_{A,sca}(h) = \pi\int_{a=0}^{\infty} a^2 Q_{sca}(a,\lambda)\,f(a,h)\,da \tag{36}$$

so

$$P_A(z') = 4\pi\left(\frac{\lambda}{2\pi}\right)^2 \frac{\int_{a=0}^{\infty} S_{11}(a,z')\,f(a,h)\,da}{\int_{a=0}^{\infty} \pi a^2 Q_{sca}(a,\lambda)\,f(a,h)\,da} \tag{37}$$

By substituting Eq. (35) into Eq. (28) we get:

$$R_{S,Lam}(\Theta) = \frac{R_0 exp\{-\tau(0)\}}{(\xi sin\Theta)^2}\left(\frac{\lambda}{2\pi}\right)^2 \int_{h=0}^{\xi}\left[\int_{a=0}^{\infty} S_{11}(a,z')f(a,h)da\right] sin^2 z'\,\mathrm{d}h\mathrm{d}S \tag{38}$$

Applying Eq. (16) to a satellite pass near the vertical of the city and assuming $\theta \approx z'$ we have:

$$tanz' = \frac{\xi sin\Theta}{h} \tag{39}$$

and

$$dh\,sin^2 z' = -\xi sin\Theta dz' \tag{40}$$

Finally, the scattered component of the radiance relative to the direct radiance of the light source is (see Eq. (6) in (Kocifaj and Bará, 2020)):

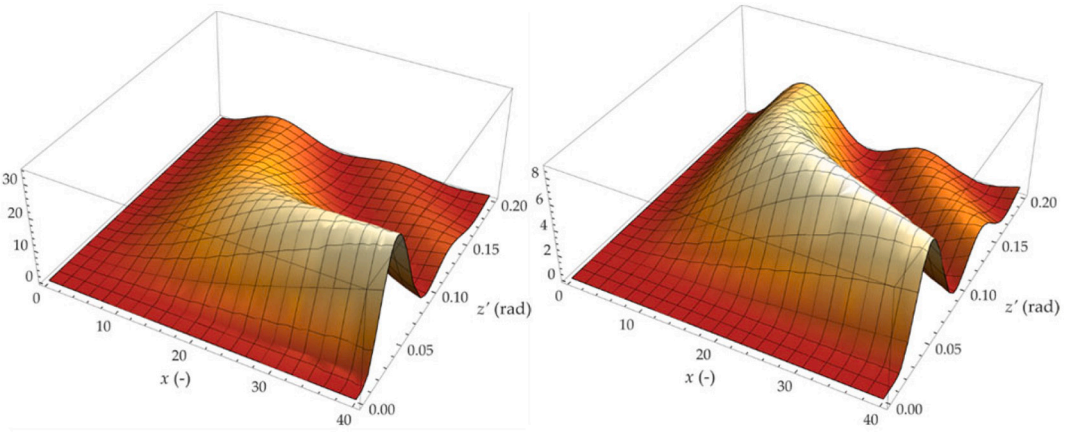

Fig. 7. The integrand in (45), for (left) $\Theta = 0.01^\circ$, and (right) $\Theta = 0.02^\circ$, $\xi \approx 829$ km, $H_A \approx 2$ km, and for z' ranging from 0 to 0.2 rad (approx. 11°).

$$\frac{R_S(\Theta_1)}{R_0 e^{-\tau(0)}} = \int_{a=0}^{\infty} f_0(a) K_{S11}(\Theta_1, a) da \tag{41}$$

where $K_{S11}(\Theta_1, x)$ has dimension of [m^3] and is equal to:

$$K_{S11}(\Theta_1, a) = 2\xi \left(\frac{\lambda}{2\pi}\right)^2 \int_{\Theta 1}^{\Theta 1+\Delta\Theta} \epsilon(\Theta) \int_{z'=0}^{\pi/2} S_{11}(a, z') exp\left(-\frac{\xi sin\Theta}{H_A tanz'}\right) dz' d\Theta \tag{42}$$

where $\Delta\Theta = \Theta_N - \Theta_1$ is specific for each nadir point (if we select other point around a city, the angles Θ will change – because city patterns usually lack any symmetry).

Eq. (41) is another main result of this work. It is a particular instance of a Fredholm integral equation of the first kind, whose inversion allows us to retrieve the size distribution function of aerosols $f_0(a)$ in the atmospheric column above the city, using as input data the available on-orbit measurements of the scattered radiance at different nadir angles, $R_S(\Theta_1)$, normalized to the direct TOA radiance received from the city, $R_0 e^{-\tau(0)}$. The success of the inversion operation strongly depends on how quickly $K_{S11}(\Theta_1, a)$ changes with a for various values of Θ_1.

A rapid estimate of the aerosol content can be made using the radiance data $R_S(\Theta_1)$ obtained at very small angles Θ_1, by applying Fraunhofer regime scattering

$$S_{11}(a, z') = \left| x^2 \frac{(1 + cosz')}{2} \frac{J_1(xsinz')}{xsinz'} \right|^2 \tag{43}$$

where $x = 2\pi a/\lambda$. After some transformations the Fredholm integral equation reduces to:

$$\frac{R_S(\Theta_1)}{R_0 e^{-\tau(0)}} = \int_{a=0}^{\infty} f_0\left(\frac{x\lambda}{2\pi}\right) K_{J1}(\Theta_1, x) dx \tag{44}$$

where the scattered radiance $R_S(\Theta_1)$ at the angular distance of Θ_1 from the city and the direct radiance of the city $R_0 e^{-\tau(0)}$ are both recorded by the satellite. The kernel of the integral in Eq. (44) has the form

$$K_{J1}(\Theta_1, x) = 2\xi \int_{\Theta 1}^{\Theta 1+\Delta\Theta} \Theta \epsilon(\Theta) L_{J1}(\Theta, x) d\Theta \tag{45}$$

where

$$L_{J1}(\Theta, x) = \frac{x^2}{\xi sin\Theta} \left(\frac{\lambda}{2\pi}\right)^3 \int_{z'=0}^{z'_0} \left[\frac{J_1(z'x)}{z'}\right]^2 exp\left(-\frac{\xi sin\Theta}{z' H_a}\right) dz' \tag{46}$$

In Fig. 7 we show the values of the integrand in (46), for $\Theta = 0.01^\circ$ and $\Theta = 0.02^\circ$, $\xi \approx 829$ km, $H_A \approx 2$ km, and z' ranging from 0 to 0.2 rad (approx. 11°). The kernel of the integral in Eq. (46) is a nonlinear function of z' and x, and in its algebraic form the integrand terms are linearly independent. For properly chosen values of Θ_1 the experimentally determined ratio $R_S(\Theta_1)/R_0 e^{-\tau(0)}$ does have sufficient information content for retrieving f_0 as a function of x.

The aerosol impact on the measured satellite radiance is thoroughly analyzed in the *Supplementary Materials* for circularly-shaped cities of various radii. There we show that the single-scattered upward radiance is a sensitive indicator of relevant aerosol properties, specifically of the particle sizes and compositions. For instance, water droplets and ammonium sulfate particles in the lower troposphere produce significantly different scattering signals (Fig. S6 in *Supplementary Materials*). This allows for using satellite radiance data to characterize and distinguish between aerosol populations in city envelopes. We also demonstrate that the aerosol contribution to the TOA radiance recorded by the satellite usually exceeds that of Rayleigh molecular scattering by one-two orders of magnitude, depending on the angular distance from the city (Fig. S3 and S5). This makes the method developed in this paper a very useful tool for tracking changes in the aerosol system in the nighttime environment.

4. Additional remarks and summary

This work provides a general framework to describe and extract the huge amount of information about the composition of the lower troposphere that is contained in multi-angle satellite measurements of the light emitted by artificial sources and scattered in the nocturnal atmosphere. The halos of light that can be observed in nighttime satellite imagery around isolated cities are described in terms of the sum of the contributions of elementary city ground elements, each one of which contributes with the spectral radiance given by Eq. (14). Particularizing this expression for near nadir-observations, and applying it for conditions in which aerosol scattering is dominant over molecular one (as in near-nadir observations from orbit), much simpler expressions can be obtained with direct application to remote sensing of different aerosol properties. In particular, we provide here a rigorous basis for the determination of the nocturnal aerosol particle number distribution function by means of the inversion of a one-dimensional Fredholm integral, whose experimental proof-of-concept was described elsewhere (Kocifaj and Bará, 2020).

The accuracy achievable in aerosol retrieval with the simplified Fredholm equation developed in this paper is limited by two practical factors. One of them is the range of validity of the assumption that the aerosol signal is dominant to such an extent that Rayleigh contributions can be neglected in the overall radiance account. We have shown that this holds fairly well for small to medium sized cities, although some

deviations could arise in case of large metropolitan areas due to the reduced ratio of aerosol to Rayleigh scattering experienced by the light emitted from city districts distant from the city border in whose angular neighborhood the near-nadir observations are made. The other is related to the assumption that outside the city borders the signal received along the satellite line of sight is composed of atmospheric scattered radiance alone, that is, that the line of sight points toward pixels of the territory where there are no artificial sources radiating significant amounts (neither directly nor after off-ground reflections). Moonlight contributions shall also be subtracted from the raw data, or either moonless nights shall be used in order to apply these equations.

This work provides the formal foundations, generalizes, and puts into a broader context the problem of remote sensing of aerosols using artificial city lights. Note finally that although the text refers explicitly to energy radiances [$W \cdot m^{-2} \cdot sr^{-1} \cdot nm^{-1}$], units in which some nighttime satellite products are provided, all concepts and formulae trivially apply for radiances expressed in terms of photon numbers [$photon \cdot s^{-1} \cdot m^{-2} \cdot sr^{-1} \cdot nm^{-1}$].

5. Conclusions

Nighttime remote sensing of atmospheric aerosols poses significant challenges in comparison with daytime sensing, most of them stemming from the lack of a suitably collimated, external reference light source. Artificial city lights, however, provide large amounts of photons that can be used to probe the neighboring atmosphere. The geometry of the scattering of light emitted from ground-based sources and detected by Earth orbiting platforms is, as expected, somewhat more involved than the one for sources located at the optical infinity. Notwithstanding that, satellite remote sensing of the diffuse halos of light surrounding cities has a huge potential for recovering important properties of the aerosol content in the lower atmosphere. We have shown in this work that under very general assumptions the aerosol particle size number distribution function can be retrieved from near-nadir multi-angle observations of the light detected in observation directions pointing out of the city but angularly close to the city borders. The high amount of information contained in these angularly resolved data sets makes it advisable to include enhanced multi-angle detection capabilities in future Earth nighttime observation missions.

Author contributions

Both authors contributed equally to the research performed, and both wrote the paper.

Funding

This work was supported by the Slovak Research and Development Agency (grant number APVV-18-0014). SB acknowledges partial funding from Xunta de Galicia (grant ED431B 2020/29).

Declaration of Competing Interest

The authors declare no conflicts of interest.

Acknowledgments

We are grateful to Igor Kohút for help with some graphical outputs. This paper is dedicated to the memory of Dr. Michael I. Mishchenko, our friend and a distinguished scientist who is known worldwide from his pioneering works on light scattering by small particles.

Appendix A. Supplementary data

Supplementary data to this article can be found online at https://doi.org/10.1016/j.atmosres.2021.105969.

References

Aptowicz, K.B., Pan, Y.L., Martin, S.D., Fernandez, E., Chang, R.K., Pinnick, R.G., 2013. Decomposition of atmospheric aerosol phase function by particle size and asphericity from measurements of single particle optical scattering patterns. J. Quant. Spectrosc. Radiat. Transf. 131, 13–23. https://doi.org/10.1016/j.jqsrt.2013.03.020.

Aznay, O., Santer, R., Zagolski, F., 2014. Validation of atmospheric scattering functions used in atmospheric correction over the ocean. Int. J. Remote Sens. 35, 4984–5003. https://doi.org/10.1080/01431161.2014.933282.

Deirmendjian, D., 1969. Electromagnetic Scattering on Spherical Polydispersions. American Elsevier Publishing Company, Inc., New York.

Dhar, P., Banik, T., De, B.K., Gogoi, M.M., Babu, S.S., Guha, A., 2018. Study of aerosol types and seasonal sources using wavelength dependent Ångström exponent over North-East India: Ground-based measurement and satellite remote sensing. Adv. Space Res. 62, 1049–1064. https://doi.org/10.1016/j.asr.2018.06.017.

Dubovik, O., Li, Z., Mishchenko, M.I., Tanré, D., Karol, Y., Bojkov, B., Cairns, B., Diner, D.J., Espinosa, W.R., Goloub, P., Gu, X., Hasekamp, O., Hong, J., Hou, W., Knobelspiesse, K.D., Landgraf, J., Li, L., Litvinov, P., Liu, Y., Lopatin, A., Marbach, T., Maring, H., Martins, V., Meijer, Y., Milinevsky, G., Mukai, S., Parol, F., Qiao, Y., Remer, L., Rietjens, J., Sano, I., Stammes, P., Stamnes, S., Sun, X., Tabary, P., Travis, L.D., Waquet, F., Xu, F., Yan, C., Yin, D., 2019. Polarimetric remote sensing of atmospheric aerosols: instruments, methodologies, results, and perspectives. J. Quant. Spectrosc. Radiat. Transf. 224, 474–511. https://doi.org/10.1016/j.jqsrt.2018.11.024.

Hartley, W.S., Hobbs, P.V., 2001. An aerosol model and aerosol-induced changes in the clear-sky albedo off the east coast of the United States. J. Geophys. Res. 106, 9733–9748. https://doi.org/10.1029/2001JD900025.

Horvath, H., Arboledas, L.A., Olmo, F.J., Jovanović, O., Gangl, M., Kaller, W., Sánchez, C., Sauerzopf, H., Seidl, S., 2002. Optical characteristics of the aerosol in Spain and Austria and its effect on radiative forcing. J. Geophys. Res. 107 (D19), 4386. https://doi.org/10.1029/2001JD001472.

Johnson, R.S., Zhang, J., Hyer, E.J., Miller, S.D., Reid, J.S., 2013. Preliminary investigations toward nighttime aerosol optical depth retrievals from the VIIRS Day/Night Band. Atmos. Meas. Tech. 6, 1245–1255. https://doi.org/10.5194/amt-6-1245-2013.

Kocifaj, M., 2007. Light-pollution model for cloudy and cloudless night skies with ground-based light sources. Appl. Opt. 46, 3013–3022. https://doi.org/10.1364/AO.46.003013.

Kocifaj, M., 2018. Multiple scattering contribution to the diffuse light of a night sky: A model which embraces all orders of scattering. J. Quant. Spectrosc. Radiat. Transf. 206, 260–272. https://doi.org/10.1016/j.jqsrt.2017.11.020.

Kocifaj, M., Bará, S., 2020. Aerosol characterization using satellite remote sensing of light pollution sources at night. Mon. Not. R. Astron. Soc. Lett. 495, L76–L80. https://doi.org/10.1093/mnrasl/slaa060.

Krueger, B.J., Grassian, V.H., Cowin, J.P., Laskin, A., 2004. Heterogeneous chemistry of individual mineral dust particles from different dust source regions: the importance of particle mineralogy. Atmos. Environ. 36, 6253–6261. https://doi.org/10.1016/j.atmosenv.2004.07.010.

Lee, K.-M., Choi, H., Kim, J., 2020. Refractive index for Asian dust in the ultraviolet-visible region determined from compositional analysis and validated with OMI Observations. J. Geophys. Res.-Atmos. 125 https://doi.org/10.1029/2019JD030629 e2019JD030629.

Levin, N., Kyba, C.C.M., Zhang, Q., Sánchez de Miguel, A., Román, M.O., Li, X., Portnov, B.A., Molthan, A.L., Jechow, A., Miller, S.D., Wang, Z., Shrestha, R.M., Elvidge, C.D., 2020. Remote sensing of night lights: A review and an outlook for the future. Remote Sens. Environ. 237, 111443 https://doi.org/10.1016/j.rse.2019.111443.

Liu, H., Pinker, R.T., Chin, M., Holben, B., Remer, L., 2008. Synthesis of information on aerosol optical properties. J. Geophys. Res. 113, D07206. https://doi.org/10.1029/2007JD008735.

McCartney, E.J., 1977. Optics of the Atmosphere. John Wiley & Sons, Chichester.

Mishchenko, M.I., Cairns, B., Chowdhary, J., Geogdzhayev, I.V., Liu, L., Travis, L.D., 2005. Remote sensing of terrestrial tropospheric aerosols from aircraft and satellites. J. Phys. Conf. Ser. 6, 73–89. https://doi.org/10.1088/1742-6596/6/1/005.

Moosmüller, H., Ogren, J.A., 2017. Parameterization of the aerosol upscatter fraction as function of the backscatter fraction and their relationships to the asymmetry parameter for radiative transfer calculations. Atmosphere 8 (133). https://doi.org/10.3390/atmos8080133.

Pandolfi, M., et al., 2018. A European aerosol phenomenology – 6: scattering properties of atmospheric aerosol particles from 28 ACTRIS sites. Atmos. Chem. Phys. 18, 7877–7911. https://doi.org/10.5194/acp-18-7877-2018.

Rodrıguez, S., Querol, X., Alastuey, A., Viana, M.-M., Alarcón, M., Mantilla, E., Ruiz, C. R., 2004. Comparative PM10–PM2.5 source contribution study at rural, urban and industrial sites during PM episodes in Eastern Spain. Sci. Total Environ. 328, 95–113. https://doi.org/10.1016/S0048-9697(03)00411-X.

Sánchez de Miguel, A., Kyba, C.C.M., Zamorano, J., Gallego, J., Gaston, K.J., 2020. The nature of the diffuse light near cities detected in nighttime satellite imagery. Sci. Rep. 10, 7829. https://doi.org/10.1038/s41598-020-64673-2.

Sobolev, V.V., 1975. Light Scattering in Planetary Atmospheres. Pergamon Press, Oxford, New York, Toronto, Sydney, Braunschweig.

Sogacheva, L., Popp, T., Sayer, A.M., Dubovik, O., Garay, M., Heckel, A., Hsu, N.C., Jethva, H., Kahn, R., Kolmonen, P., Kosmale, M., de Leeuw, G., Levy, R., Lytvynov, P., Lyapustin, A., North, P., Torres, O., Arola, A., 2020. Merging regional and global aerosol optical depth records from major available satellite products. Atmos. Chem. Phys. 20, 2031–2056. https://doi.org/10.5194/acp-20-2031-2020.

Spurr, R.J.D., 2006. VLIDORT: a linearized pseudo-spherical vector discrete ordinate radiative transfer code for forward model and retrieval studies in multilayer multiple scattering media. J. Quant. Spectrosc. Radiat. Transfer. 102, 316–342. https://doi.org/10.1016/j.jqsrt.2006.05.005.

Videen, G., Pinnick, R.G., Ngo, D., Fu, Q., Chýlek, P., 1998. Asymmetry parameter and aggregate particles. Appl. Opt. 37, 1104–1109. https://doi.org/10.1364/ao.37.001104.

Wang, J., Zhou, M., Xu, X., Roudini, S., Sander, S.P., Pongetti, T.J., Miller, S.D., Reid, J. S., Hyer, E.J., Spurr, R., 2020. Development of a nighttime shortwave radiative transfer model for remote sensing of nocturnal aerosols and fires from VIIRS. Remote Sens. Environ. 241, 111727 https://doi.org/10.1016/j.rse.2020.111727.

Zhang, J., Reid, J.S., Turk, J., Miller, S., 2008. Strategy for studying nocturnal aerosol optical depth using artificial lights. Int. J. Remote Sens. 29, 4599–4613. https://doi.org/10.1080/01431160802020528.

Zhang, H., et al., 2012. Simulation of direct radiative forcing of aerosols and their effects on East Asian climate using an interactive AGCM-aerosol coupled system. Clim. Dyn. 38, 1675–1693. https://doi.org/10.1007/s00382-011-1131-0.

Zhang, Y., Li, Z., Bai, K., Wei, Y., Xie, Y., Zhang, Y., Ou, Y., Cohen, J., Zhang, Y., Peng, Z., Zhang, X., Cheng, C., Hong, J., Xu, H., Guang, J., Lv, Y., Li, K., Li, D., 2021. Satellite remote sensing of atmospheric particulate matter mass concentration: advances, challenges, and perspectives. Fundamental Res. 1, 240–258. https://doi.org/10.1016/j.fmre.2021.04.007.